Inorganic Chemistry
Article

Inorg. Chem. **2010**, *49*, 1449–1457 **1449**
DOI: 10.1021/ic901682x

Shape-Controllable Synthesis and Morphology-Dependent Luminescence Properties of GaOOH:Dy^{3+} and β-Ga_2O_3:Dy^{3+}

Guogang Li,[†,‡] Chong Peng,[†,‡] Chunxia Li,[†] Piaoping Yang,[†] Zhiyao Hou,[†] Yong Fan,[†] Ziyong Cheng, and Jun Lin*[,†]

[†] *State Key Laboratory of Rare Earth Resource Utilization, Changchun Institute of Applied Chemistry, Chinese Academy of Sciences, Changchun 130022, People's Republic of China, and* [‡] *Graduate University of the Chinese Academy of Sciences, Beijing 100049, People's Republic of China*

Received August 24, 2009

Dy^{3+}-doped gallium oxide hydroxides (GaOOH:Dy^{3+}) with various morphologies (submicrospindles, submicroellipsoids, 3D hierarchical microspheres) were synthesized by a facile soft-chemical method. After annealing at 1000 °C, the GaOOH:Dy^{3+} precursor was easily converted to β-Ga_2O_3:Dy^{3+} phosphors which kept their original morphologies. The as-prepared GaOOH:Dy^{3+} and β-Ga_2O_3:Dy^{3+} products were characterized using X-ray diffraction (XRD), field-emission scanning electron microscopy (FESEM), low- to high-resolution transmission electron microscopy (TEM), selected area electron diffraction (SAED), photoluminescence (PL) spectra, cathodoluminescence (CL) spectra, and quantum yield (QY). With an increase in pH from 4 to 9, the morphology of GaOOH:Dy^{3+} varied from submicrospindles to 3D hierarchical microspheres of self-assembled nanoparticles. A possible mechanism for the formation of various morphologies of GaOOH:Dy^{3+} and β-Ga_2O_3:Dy^{3+} was proposed. Under ultraviolet and low-voltage electron beam excitation, the pure β-Ga_2O_3 samples exhibit a blue emission with a maximum at 438 nm originating from the GaO_6 groups, while the β-Ga_2O_3:Dy^{3+} samples show the characteristic emission of Dy^{3+} corresponding to $^4F_{9/2} \rightarrow {}^6H_{15/2,\ 13/2}$ transitions due to an efficient energy transfer from β-Ga_2O_3 to Dy^{3+}. A simple model was proposed to explain the energy transfer process and luminescence mechanism. Furthermore, the dependence of luminescence intensity on the morphology has been investigated in detail. Under 257 nm UV and electron beam excitation, the β-Ga_2O_3:Dy^{3+} phosphor with a submicroellipsoid shape shows the highest relative emission intensity and quantum yield compared with other morphologies, and the obtained phosphors have potential applications in the areas of fluorescent lamps and field emission displays (FEDs).

1. Introduction

Recently, the shape-controllable synthesis of inorganic nano-, submicro-, and microcrystals has aroused considerable attention owing to their useful properties, which allow for applications in optics, electrics, magnetics, and optoelectronic devices.[1,2] The composition, morphology, and size of these materials are important factors that dictate their characteristic properties.[3−6] Therefore, in the development of a synthetic method to generate nano-/microstructures, the most important issue to be addressed is simultaneous control over dimensions, morphology, and monodispersity. In the past decade, many efforts have been made to explore excellent approaches for the fabrication of a variety of inorganic crystals to enhance their performance in currently existing applications. Among them, the soft-chemical method has been proved to be one of the most effective and convenient approaches in preparing various inorganic materials with diversely controllable morphologies and architectures in terms of cost and potential for large-scale production. Generally, it can be classified into two types: the first one is the template method, which employs either hard templates such as polymeric core supports and sacrificial metal substrates or soft templates such as micelles in emulsions or ionic liquids.[7] However, the addition of a template to the reaction system involves a complicated process and may result in impurities due to the incomplete removal of the template.

---

*To whom correspondence should be addressed. E-mail: jlin@ciac.jl.cn.

[1] Im, S. H.; Lee, Y. T.; Wiely, B.; Xia, Y. N. *Angew. Chem., Int. Ed.* **2005**, *44*, 2154.

[2] Cheng, F. C.; Zhao, J. Z.; Li, C. S.; Ma, H.; Chen, J.; Shen, P. W. *Inorg. Chem.* **2006**, *45*, 2038.

[3] (a) Alivisatos, A. P. *Science* **1996**, *271*, 933. (b) Xia, Y. N.; Yang, P. D.; Sun, Y. G.; Wu, Y. Y.; Mayers, B.; Gates, B.; Yin, Y. D.; Kim, F.; Yan, Y. Q. *Adv. Mater.* **2003**, *15*, 353. (c) Burda, C.; Chen, X.; Narayanan, R.; El-Sayed, M. A. *Chem. Rev.* **2005**, *105*, 1025. (d) Zhang, J.; Li, X.; Sun, X.; Li, Y. *J. Phys. Chem. B* **2005**, *109*, 12544.

[4] Dong, H.; Li, X. J.; Peng, Q.; Wang, X.; Chen, J. P.; Li, Y. D. *Angew. Chem., Int. Ed.* **2005**, *44*, 2782.

[5] Sun, S.; Murray, C. B.; Weller, D.; Folks, L.; Moser, A. *Science* **2000**, *287*, 1989.

[6] Mokari, T.; Zhang, M.; Yang, P. *J. Am. Chem. Soc.* **2007**, *129*, 9864.

[7] (a) Han, W.; Fan, S.; Li, Q.; Hu, Y. *Science* **1997**, *277*, 1287. (b) Yada, M.; Mihara, M.; Mouri, S.; Kuroki, M.; Kijima, T. *Adv. Mater.* **2002**, *14*, 309. (c) Sun, X. M.; Li, Y. D. *Angew. Chem., Int. Ed.* **2004**, *43*, 3827. (d) Jacob, D. S.; Bitton, L.; Grinblat, J.; Felner, I.; Koltypin, Y.; Gedanken, A. *Chem. Mater.* **2006**, *18*, 3162.

The other method are template-free methods such as homogeneous precipitation, hydrothermal/solvothermal processes, and so on, which can overcome the above difficulties by the use of simple, one-step, effective solution-phase methods for fabricating novel assemblies of the inorganic materials under template-free conditions or without the aid of other techniques.[8] Therefore, the latter method seems to be more attractive and promising, owing to its higher yield and simplicity.

Field emission displays (FEDs) are considered as one of the most promising next-generation flat panel display techniques due to their potential to provide a display with a thin panel, self-emission, wide viewing, quick response time, high brightness, high contrast ratio, light weight, and low power consumption.[9,10] In the development of FEDs, one of the most important factors is to develop highly efficient phosphors at low electron excitation voltages (≤ 5 kV) and high current densities (10−100 $\mu A/cm^2$).[11] Semiconducting oxide based phosphors have been found to be one of the optimal candidates, as they are sufficiently conductive to overcome the charge buildup on phosphor surfaces, in addition to their thermal and chemical stability.[12,13] β-Ga_2O_3 is a wide band gap (4.9 eV) semiconductor that has been used as a visible blue-green light emitter.[14,15] Simultaneously, it has also been used as a phosphor host material for application in thin-film electroluminescent and cathodoluminescent displays.[16,17] On the other hand, rare earth ions have been playing an important role in modern lighting and display fields due to the abundant emission colors based on their 4f → 4f or 5d → 4f transitions.[18,19] The emission of Dy^{3+} is mainly due to transitions of $^4F_{9/2}$−$^6H_{15/2}$ in the blue region (470−500 nm) and $^4F_{9/2}$−$^6H_{13/2}$ in the yellow-orange region (570−600 nm). Moreover, at a suitable yellow-to-blue intensity ratio, Dy^{3+} will emit white light.[20a] However, unlike the most frequently used Eu^{3+} and Tb^{3+} (in oxide hosts), which have an allowed charge-transfer absorption band (CTB) or $4f^8$−$4f^75d$ absorption band in the UV region, respectively, the excitation spectrum of Dy^{3+} consists of only narrow f−f transition lines with low oscillator strength (10^{-6}) due to their forbidden features by the parity selection rule from 300 to 500 nm (both the CTB and $4f^9$−$4f^85d$ band of Dy^{3+} are located below 200 nm).[18,21] Host sensitization for Dy^{3+} ions, i.e., efficient energy transfer from the host to Dy^{3+} ions, is one of the most significant routes for realizing the efficient emission of Dy^{3+} ions, such as $YVO_4:Dy^{3+}$.[22]

Herein, we demonstrate a facile homogeneous precipitation process to fabricate $GaOOH:Dy^{3+}$ precursors with various well-defined morphologies, including submicrospindles, submicroellipsoids, and 3D hierarchical microspheres. The experimental results indicate that the pH values of the initial reaction systems are critical factors for determining the architectural features of the final products. The morphological evolution and the growth mechanism for the synthesized $GaOOH:Dy^{3+}$ precursor under different pH conditions has been studied in detail. After heat treatment at 1000 °C, the $GaOOH:Dy^{3+}$ species were successfully converted to β-$Ga_2O_3:Dy^{3+}$ which kept their original morphologies. The photoluminescent (PL) and cathodoluminescent (CL) properties for these β-$Ga_2O_3:Dy^{3+}$ samples with various morphologies have been investigated in detail.

2. Experimental Section

2.1. Materials. The starting materials were commercial Ga_2O_3 (99.99%, Shanghai Sinopharm Chemical Reagent Co., Ltd.), Dy_2O_3 (99.999%, Science and Technology Parent Company of Changchun Institute of Applied Chemistry), and HCl and urea (Beijing Chemical Co.). All chemicals were analytical grade reagents and used directly without further purification.

2.2. Preparation. In a typical synthesis procedure, proper amounts of Ga_2O_3 and Dy_2O_3 were dissolved in dilute HCl followed by addition of distilled water to reach a total volume of 500 mL. In each case, the total concentration of Ga^{3+} and Dy^{3+} was constantly kept at 0.015 mol/L and 0.25 mol of urea used as the precipitator, and the source of OH^- was added into the solution to keep the concentration at 0.5 mol/L. The mixed solution, contained in a beaker wrapped with polyethylene film, was first homogenized under magnetic stirring at room temperature for 2 h and was then heated on a hot plate with strong stirring to reach 90 °C within 60 min. After reaction at 90 °C for 4 h, the suspension was cooled to room temperature naturally and the resulting precipitates were separated by centrifugation, washed with deionized water and anhydrous ethanol in sequence four times, and then dried in air at 90 °C for 24 h. The as-prepared precursors were denoted as **P1−P4**, in which the pH values of the initial solutions were adjusted with 1 mol/L HCl and 25% ammonia to 4, 6, 7, and 9, respectively. The resulting β-$Ga_2O_3:Dy^{3+}$ products were retrieved through a calcination treatment of $GaOOH:Dy^{3+}$ at 1000 °C for 4 h in air, which were denoted as **P1′−P4′**, corresponding to the **P1−P4** precursors, respectively. It should be stated that the Dy^{3+} substitutes for Ga^{3+} in $GaOOH:Dy^{3+}$ and β-Ga_2O_3: Dy^{3+}, and the doping concentrations of Dy^{3+} are all depicted as mole percent of Ga^{3+}.

2.3. Characterization. Powder X-ray diffraction (XRD) measurements were performed on a D8 Focus diffractometer (Bruker) at a scanning rate of 15°/min in the 2θ range from 10 to 80°, with graphite-monochromated Cu Ka radiation (λ = 0.154 05 nm). SEM micrographs were obtained using a field emission scanning electron microscope (FE-SEM, S-4800, Hitachi). Low- to high-resolution transmission electron microscopy (TEM) and selected area electron diffraction (SAED) patterns were performed using a FEI Tecnai G2 S-Twin instrument with a field emission gun operating at 200 kV, and images were acquired digitally on a Gatan multiople CCD camera. Photoluminescence (PL) measurements were performed on a Hitachi F-4500 spectrophotometer equipped with a 150 W

---

(8) Liu, J. P.; Huang, X. T.; Li, Y. Y.; Sulieman, K. M.; He, X.; Sun, F. L. *Cryst. Growth Des.* **2006**, *6*, 1690.

(9) Jüstel, T.; Nikol, H.; Ronda, C. *Angew. Chem., Int. Ed.* **1998**, *37*, 3084.

(10) Hirosaki, N.; Xie, R.; Inoue, K.; Sekiguchi, T.; Dierre, B.; Tamura, K. *Appl. Phys. Lett.* **2007**, *91*, 061101.

(11) Jing, Y. D.; Zhang, F.; Summers, C. J.; Wang, Z. L. *Appl. Phys. Lett.* **1999**, *74*, 1677.

(12) Holloway, P. H. T.; Trottier, A.; Abrams, B.; Kondoleon, C.; Jones, S. L.; Sebastian, J. S.; Thomes, W. J.; Swart, H. *J. Vac. Sci. Technol. B* **1999**, *17*, 758.

(13) Yu, M.; Lin, J.; Zhou, Y. H.; Wang, S. B. *Mater. Lett.* **2002**, *56*, 1007.

(14) Ogita, M.; Saika, N.; Nakanishi, Y.; Hatanaka, Y. *Appl. Surf. Sci.* **1999**, *142*, 188.

(15) Li, Z.; De Groot, C.; Moodera, J. H. *Appl. Phys. Lett.* **2000**, *77*, 3630.

(16) Xiao, T.; Kitai, A. H.; Liu, G.; Nakua, A.; Barbier, J. *Appl. Phys. Lett.* **1998**, *72*, 3356.

(17) (a) Hao, J.; Cocivera, M. *J. Phys. D.* **2002**, *35*, 433. (b) Cao, C. B.; Chen, Z.; An, X. Q.; Zhu, H. S. *J. Phys. Chem. C* **2008**, *112*, 95.

(18) Blasse, G.; Grabmaier, B. C. *Luminescence Materials*; Springer-Verlag: Berlin, Heidelberg, 1994; Chapters 4 and 5.

(19) Tang, Y. S.; Hu, S. F.; Lin, C. C.; Bagkar, N. C.; Liu, R. S. *Appl. Phys. Lett.* **2007**, *90*, 151108.

(20) (a) Liu, X.; Lin, C.; Luo, Y.; Lin, J. *J. Electrochem. Soc.* **2007**, *154*, J21. (b) Liu, X. M.; Yu, C. C.; Li, C. X.; Lin, J. *J. Electrochem. Soc.* **2007**, *154*, 86.

(21) Loh, E. *Phys. Rev.* **1966**, *147*, 332.

(22) Sommerdijk, J. L.; Bril, A.; Hoex-Strik, F. M. J. H. *Philips Res. Rep.* **1977**, *32*, 149.

xenon lamp as the excitation source. Cathodoluminescence measurements were carried out in an ultrahigh vacuum chamber (< 10^{-8} Torr), where the phosphors were excited by an electron beam in the voltage range of 0.5−3.5 kV and different filament currents and the emission spectra were recorded using an F-4500 spectrophotometer. Photoluminescence quantum yield (QY) was measured by a C9920-02 absolute PL quantum yield measurement system from Hamamatsu. All the measurements were performed at room temperature.

3. Results and Discussion

3.1. Crystallization and Morphology of GaOOH:Dy^{3+} Precursors.

The phase purity and morphology of the studied samples were representatively investigated by applying XRD and FE-SEM on the GaOOH:3 mol % Dy^{3+} (3 mol % of Ga^{3+}) precursors. The results for other doping concentrations of Dy^{3+} in the GaOOH:x mol % Dy^{3+} (x = 0−5) system are similar to those of GaOOH: 3 mol % Dy^{3+} and will not be shown here. Figure 1 shows the XRD patterns of the GaOOH:3 mol % Dy^{3+} precursors prepared through a homogeneous precipitation process at 90 °C for 4 h under different pH conditions of (a) pH 4, (b) pH 6, (c) pH 7, and (d) pH 9, respectively. The diffraction peaks of the four samples can be easily assigned to a pure orthorhombic phase of GaOOH (space group *Pbnm* (No. 62)), which are consistent with the literature values (JCPDS No. 54-0910). No obvious shifting of peaks or second phase can be detected at the current doping level, indicating that the Dy^{3+} ions are completely dissolved in the GaOOH host lattices by substitution for the Ga^{3+}. It is worth pointing out that the XRD pattern also indicates that there is some difference in the relative intensities based on (110) and (111) for the four samples, indicating the possibility of different preferential orientation growth under different pH conditions.

The morphology and size of Dy^{3+}-doped gallium oxide hydroxide was studied by FE-SEM. Figure 2 shows the representative SEM images of GaOOH:3 mol % Dy^{3+} precursors prepared at 90 °C for 4 h in aqueous solution through a homogeneous precipitation process. Interestingly, various morphologies of GaOOH:3 mol % Dy^{3+} were synthesized simply by adjusting the pH. There were significant differences in the morphology and crystallite sizes of these GaOOH:3 mol % Dy^{3+} powders. GaOOH:3 mol % Dy^{3+} powder prepared at pH 4 (denoted as **P1**) was composed of a great deal of highly uniform submicrospindles with an average length and equator diameter of about 0.85 and 0.2 μm, respectively (Figure 2a), and the ratio of long-axis length to equator diameter ($r_{\mathrm{L/D}}$) equals 4.3. Moreover, it can be seen from the inset (a magnified view of Figure 2a) that the surfaces of submicrospindles were rough and were covered with large numbers of microcrystals, indicating that the formation of submicrospindles might be induced by stacking a great amount of nanoparticles. Powders prepared at pH 6 (**P2**) were also made up of submicrospindles, as shown in Figure 2b. However, the length and width of a single spindle became bigger, in which the average length and equator diameter increased to ~1.1 and ~0.5 μm, respectively, and the $r_{\mathrm{L/D}}$ decreased to 2.2. When the pH of the initial solution was increased from 6 to 7 (**P3**), the length of an individual particle was still ~1.1 μm, but its equator diameter increased to 0.85 μm. As a result, the $r_{\mathrm{L/D}}$ value of the **P3** sample decreased to 1.3, resulting in the products forming an ellipsoid-like morphology (Figure 2c and its inset). At pH 9 (**P4**), the average $r_{\mathrm{L/D}}$ was close to 1.0 and 3D hierarchical microspheres were obtained with an average diameter of 5.5 μm. In summary, the overall morphology changed from submicrospindles to 3D hierarchical microspheres when the pH was increased from 4 to 9. Furthermore, the length and equator diameter simultaneously increased, while the increased rate of long-axis direction was slower than that of the equator direction with an increase in the pH, which resulted in the $r_{\mathrm{L/D}}$ continuously decreasing and the morphology trending to form a sphere-like morphology. All the experimental parameters were invariable in the experimental process except for the pH values; therefore, the pH values play a key role in the formation of various morphologies of GaOOH: 3 mol % Dy^{3+} precursors. The experimental conditions, morphologies, sizes, and ratio of long-axis length and equator diameter are summarized in Table 1.

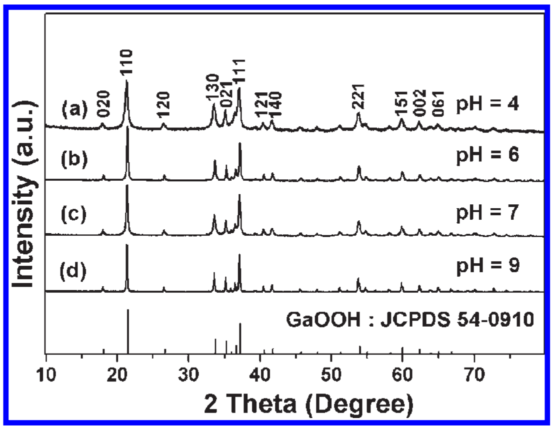

Figure 1. XRD patterns of GaOOH:3 mol % Dy^{3+} precursors prepared at different pH values: (a) pH 4; (b) pH 6; (c) pH = 7; (d) pH 9. The standard data for GaOOH (JCPDS 54-0910) are shown as a reference.

To examine the typical direction of growth for spindle-like GaOOH:3 mol % Dy^{3+}, the **P1** sample was further studied by using high-resolution transmission electron microscopy (HRTEM), and the results are shown in Figure 3b. The spacing of the lattice planes along the length of the submicrospindle was 0.41 nm, which corresponds to an interplanar spacing of the (110) plane of orthorhombic GaOOH. The corresponding SAED pattern (Figure 3b, inset) reveals a single-crystal structure of the sample, and the diffraction spots can be indexed to a pure orthorhombic phase of GaOOH. The crystal orientations of the submicrospindle along the length and width are determined to be [001] and [100], respectively, as illustrated in the inset of Figure 3b. In agreement with the previous reports by Huang and Qian,[23,24] the preferential growth direction of GaOOH:3 mol % Dy^{3+} submicrospindles is along the c axis.

To investigate the formation mechanism of various morphologies of GaOOH:Dy^{3+} prepared at different pH values, the products formed at different growth stages were collected for SEM and TEM analyses. On the basis

---

(23) Huang, C. C.; Yeh, C. S.; Ho, C. J. *J. Phys. Chem. B* **2004**, *108*, 4940.

(24) Qian, H. S.; Gun, W. P.; Zhang, Y. X.; Lin, G. F.; Zheng, J. W.; Xu, R. *Cryst. Growth Des.* **2008**, *8*, 1282.

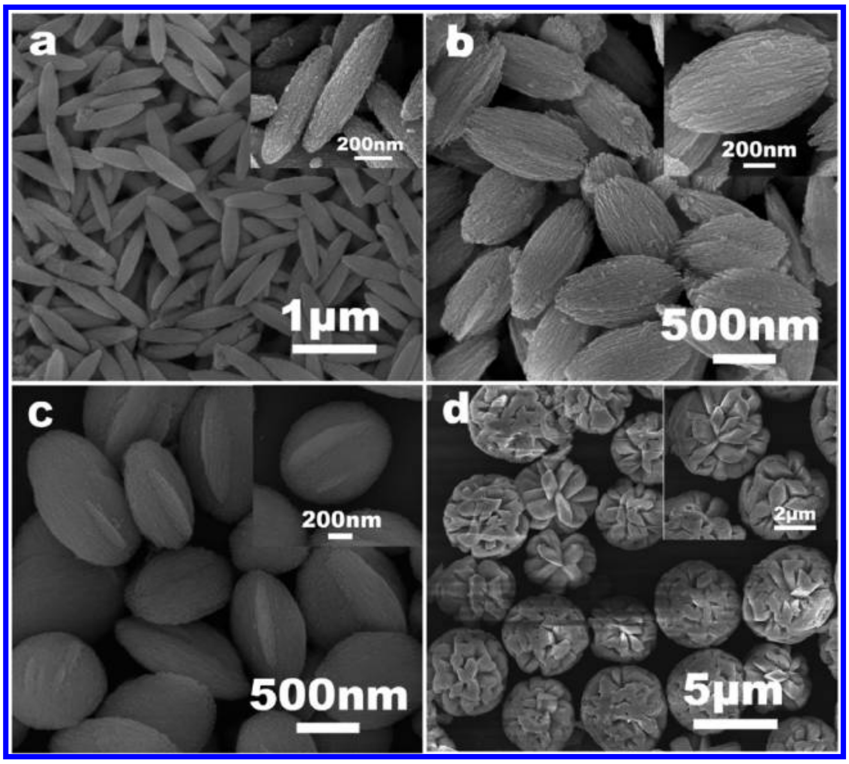

Figure 2. Typical FE-SEM images of GaOOH:3 mol % Dy^{3+} precursors prepared at different pH values: (a) pH 4, (b) pH 6; (c) pH 7; (d) pH 9. The insets are corresponding magnified micrographs.

Table 1. Summary of the Experimental Conditions, Morphologies, Sizes, and Ratio of Long-Axis Length and Equator Diameter ($r_{L/D}$) of GaOOH:3 mol % Dy^{3+} Samples

sample	pH	morphology	length (μm)	diameter (μm)	$r_{L/D}$
P1	4	submicrospindles	0.85	0.2	4.3
P2	6	submicrospindles	1.1	0.5	2.2
P3	7	submicroellipsoids	1.1	0.85	1.3
P4	9	3D hierarchical microspheres		5.5	~1.0

of these experimental results and the observation of the early growth stage, the mechanisms of the formation and evolution of the various morphologies of GaOOH:Dy^{3+} prepared at different pH values are proposed as follows:

(I). Formation of Amorphous Spherical Nanoparticles. It was found that a white precipitate comprised of aggregates of amorphous spherical nanoparticles of ~10 nm appeared after the reaction of $GaCl_3$, $DyCl_3$, and $CO(NH_2)_2$ solution at 90 °C for 10 min, as shown in Figure 4a. On aging of the mixed solution at 90 °C for 30 min, some spindlelike nanoparticles of 700−900 nm in length and 150−300 nm in width were formed together with an amorphous phase (Figure 4b). However, on aging at 90 °C for 1 h, the amorphous phase disappeared and almost totally converted to highly uniform and monodisperse submicrospidles (Figure 4c). Moreover, the precipitate was composed of Ga, O, Dy, and a small quantity of C impurity (resulting from $CO(NH_2)_2$), as determined by EDX analysis (H cannot be detected by this equipment) (Figure 4d). Therefore, it is thought that the final spindles, ellipsoids, and 3D hierarchical sphere morphologies were produced from these amorphous nanoparticles, which formed during the early growth stage.

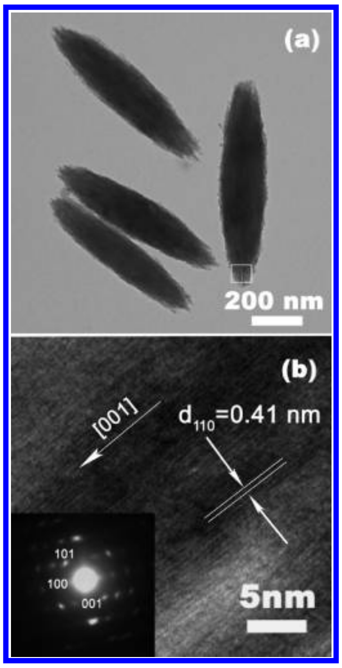

Figure 3. (a) TEM image of GaOOH:3 mol % Dy^{3+} submicrospindles prepared at 90 °C under pH 4 (**P1**); (b) the corresponding HRTEM image and SAED pattern obtained from a head region.

(II). Crystallization, Growth, and Aggregation. Figure 5 shows typical FTIR spectra of GaOOH:Dy^{3+} powders prepared at different pHs. Except for the amorphous precipitates, the FTIR spectra of all the powders are approximately identical. The IR spectra of **P1**−**P4** samples reveal a broad H−O−H stretching band at around 3410 cm^{-1} and an OH bending at 1637 cm^{-1}. On the other hand, the bands at 2032 and 1939 cm^{-1}, together with the

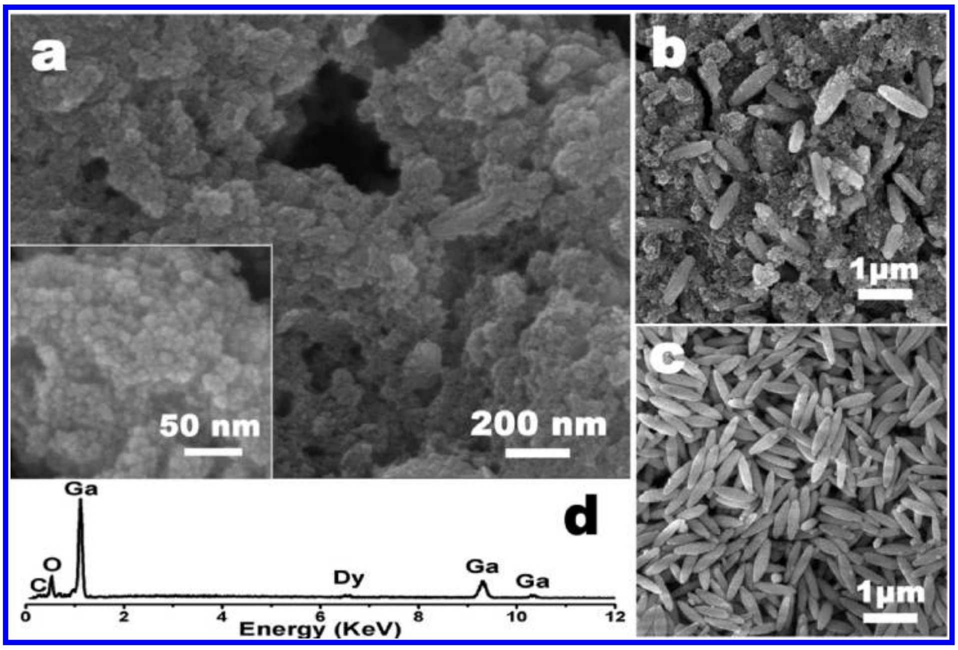

Figure 4. Typical SEM images (a) of the precipitated amorphous powder (after mixing the initial solutions at a pH of 4 and heating to 90 °C for 10 min) and on aging at 90 °C for (b) 30 min and (c) 1 h. (d) EDX spectrum of the **P1** sample.

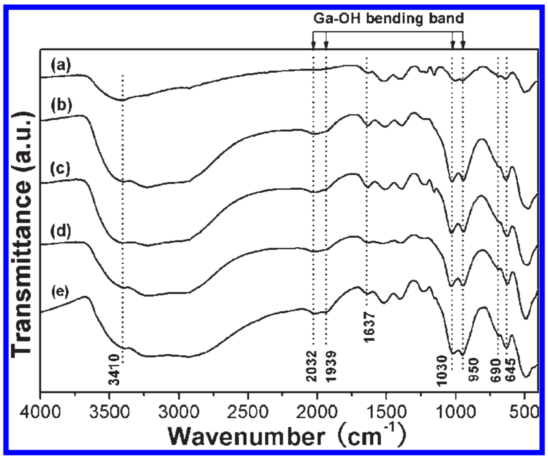

Figure 5. FTIR spectra of GaOOH:Dy^{3+} powders prepared at various pHs: (a) amorphous precipitate; (b) pH 4 (**P1**); (c) pH 6 (**P2**); (d) pH 7 (**P3**); (e) pH 9 (**P4**).

bands at 1030 and 950 cm^{-1}, are assigned to constitutional Ga−OH bending bands and their overtones, respectively, which is consistent with prior research.[25] Moreover, the bands (including those at 690 and 645 cm^{-1}) appearing within the range 1200−600 cm^{-1} are characteristic M−OH deformation bands seen in hydroxo complexes.[26] It is noticed that the lattice OH vibration modes were not observed for the amorphous powder, which implies that the adsorption of OH^- ions onto the surface is necessary for the crystallization and growth of GaOOH:Dy^{3+}. These observations indicate that OH^- ions play an important role in the changing morphology that occurs during the crystallization and growth process.

Therefore, it is understood that at low pH (such as pH 4, acidic environment, low OH^- ion concentration), the probability of the adsorption of OH^- ions onto the surface of the amorphous particles was limited and preferentially resulted in anisotropic growth: i.e., certain facets with relatively higher free energies will preferentially form the active sites and show higher growth rate. Herein the facet (001) of the GaOOH crystal has a preferential absorption of OH^- ions and higher growth rate than other crystallite facets due to the different surface energies of crystallite facets. These particles then grew along one orientation (001) at a higher rate to give good-quality crystalline submicrospindles with a length/diameter ratio (Figure 4c) higher than that of the others. Such a mechanism of the formation of the submicrospindles is consistent with the GaOOH nanorods reported by Penn and Liu.[27−31] On the other hand, when the pH of the initial solution is increased, each facet of the crystallite had almost the same probability to generate active sites due to the homogeneous absorption of OH^-, which resulted in isotropic growth: i.e., individual crystallites had lower length/diameter ratios and grew into ellipsoids or spheres, as shown in Figure S1 (Supporting Information). Figure S1b shows the morphology of **P4** (pH 9) powder at the early growth stage (after 1 h). It can be seen that an intermediate structure mixing with branched and crossed spindlelike morphology forms. These intermediates suggest that spindles are formed first, and the spindles can aggregate and grow further, resulting in a branched and crossed morphology. These branched

---

(25) (a) Sato, T.; Nakamura, T. *J. Chem. Tech. Biotechnol.* **1982**, *32*, 469. (b) Cüneyt Tas, A.; Majewski, P. J.; Aldinger, F. *J. Am. Ceram. Soc.* **2002**, *85*, 1421.

(26) Socrates, G. *Infrared Characteristic Group Frequencies*; Wiley: New York, 1994; p 224.

(27) Liu, G. C.; Duan, X. C.; Li, H. B.; Liang, D. W. *Mater. Chem. Phys.* **2008**, *110*, 206.

(28) (a) Welch, J. F.; Banfield, S. A.; Zhang, H.; Ebert, T. T.; Penn, R. L. *Science* **2000**, *289*, 751. (b) Penn, R. L.; Banfield, J. F. *Science* **1998**, *281*, 969.

(29) Zhang, J.; Liu, Z. G.; Lin, C. K.; Lin, J. *J. Cryst. Growth* **2005**, *280*, 99.

(30) Li, W. J.; Shi, E. W.; Zhong, W. Z.; Yin, Z. W. *J. Cryst. Growth* **1999**, *203*, 186.

(31) Patungwasa, W.; Hodak, J. H. *Mater. Chem. Phys.* **2008**, *108*, 45.

Scheme 1. Schematic Illustration of the Formation and Morphology Evolution Mechanism GaOOH:Dy^{3+} Based upon Initial pH[a]

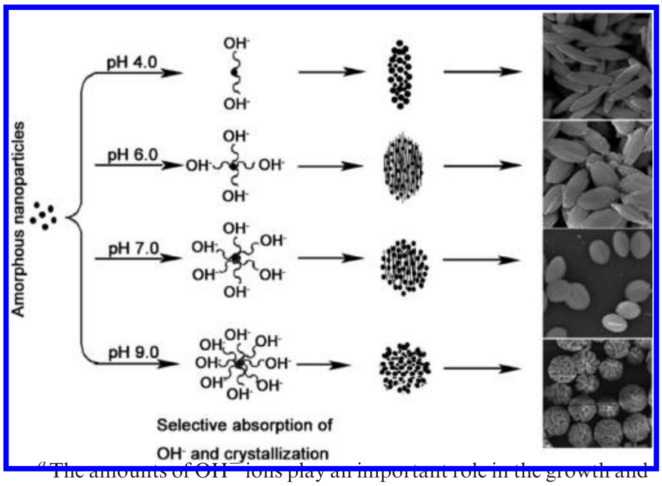

[a] The amounts of OH^- ions play an important role in the growth and aggregation process.

and crossed intermediates further grow into 3D hierarchical microspheres when the reaction proceeds for a long time.

In summary, it is obvious that the OH^- ions play important roles in the shape of the crystallites and the aggregation process, respectively. On the basis of the above results, a schematic illustration of the formation and subsequent evolution of the morphology of GaOOH at different pH values is presented in Scheme 1.

3.2. β-Ga_2O_3:Dy^{3+}. The most convenient and frequently used route for large-scale synthesis of gallium oxide (Ga_2O_3) is thermal decomposition of gallium oxyhydroxide (GaOOH), which can be readily prepared by soft-chemical methods.[24,32] Generally, the transformation from gallium oxyhydroxide to gallium oxide is related to the types and properties of the gallium precursor,[23,34] and the formation of β-Ga_2O_3 needs a higher temperature (T > 870 °C) calcination.[33] In our work, GaOOH:3 mol % Dy^{3+} species with various morphologies (shown in Figure 2) were used as the precursors. After the precursors were calcined at 1000 °C for 2 h, β-Ga_2O_3: 3 mol % Dy^{3+} (Dy^{3+} instead of Ga^{3+}) products were obtained, as confirmed by XRD results in Figure 6. In general, the X-ray diffraction peaks of the as-formed products are in agreement with the monoclinic phase of Ga_2O_3 (space group $C2/m$ (No. 12)) according to the JCPDS file No. 41-1103 except for a minor impurity peak at ~32° for **P2′**−**P4′** samples and at ~28° for **P1′** and **P2′** samples. The former can be attributed to the $Dy_3Ga_5O_{12}$ phase (JCPDS 13-0426) and the latter possibly results from the Ga_2O_3 phase (JCPDS 06-0509).[20b] No obvious shifting of peaks can be detected at the current doping level, indicating that the GaOOH:3 mol % Dy^{3+} precursors were completely converted to β-Ga_2O_3:3 mol % Dy^{3+} and Dy^{3+} ions were also completely dissolved in the Ga_2O_3 host lattices by substitution for the Ga^{3+} ions.

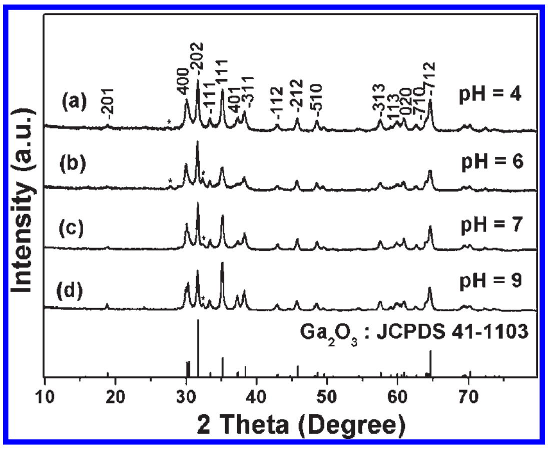

Figure 6. XRD patterns of β-Ga_2O_3:3 mol % Dy^{3+} powders with various morphologies annealed at 1000 °C for 2 h: (a) pH 4; (b) pH 6; (c) pH 7; (d) pH 9. The standard data for Ga_2O_3 (JCPDS 41-1103) are shown as a reference.

Figure S2 (Supporting Information) shows typical SEM images of β-Ga_2O_3:3 mol % Dy^{3+} products calcined at 1000 °C. It can be seen that the β-Ga_2O_3:0.03Dy^{3+} products inherited their parents' morphology, but their size is slightly shrunk in comparison with that of the gallium oxide hydroxide precursors. Such a transformation was common for obtaining metal oxide.[35,36] The morphologies were maintained due to the higher activation energies needed for the collapse of these structures.[37] The EDX was used to further characterize the chemical composition of the as-prepared product. The EDX spectrum (Figure S2e) shows the presence of Ga, O, and Dy, which matches well with that of gallium oxide β-Ga_2O_3:Dy^{3+}. The EDX result gives further support for the above XRD analysis. To further study the fine structure of the above β-Ga_2O_3: Dy^{3+} samples, TEM and HR-TEM were representatively performed on the **P1′** and **P4′** samples, respectively, as shown in Figure 7. The HRTEM images of a part of a single submicrospindle (Figure 7b) and 3D hierarchical microsphere (Figure 7d) show several lattice planes with perfect crystallinity. The lattice fringes of the **P1′** sample show the imaging characteristics of the monoclinic Ga_2O_3 crystal, in which the d spacing of 0.298 nm corresponds to the distance between the (400) planes. The d spacings of **P2′** and **P3′** samples are 0.294 and 0.296 nm, respectively, which can also be assigned to the distance between the (400) planes as shown in Figure S3 (Supporting Information). However, the HRTEM result

---

(32) (a) Laubengayer, A. W.; Engle, H. R. *J. Am. Chem. Soc.* **1939**, *61*, 121. (b) Sato, T.; Nakamura, T. *Thermochim. Acta* **1982**, *53*, 281.

(33) Fleischer, M.; Höllbauer, L.; Born, E.; Meixner, H. *J. Am. Ceram. Soc.* **1997**, *80*, 2121.

(34) (a) Roy, R.; Hill, V. G.; Osborn, E. F. *J. Am. Chem. Soc.* **1952**, *74*, 719. (b) Ristic, M.; Popovic, S.; Music, S. *Mater. Lett.* **2005**, *59*, 1227.

(35) (a) Xu, A. W.; Fang, Y. P.; You, L. P.; Liu, H. Q. *J. Am. Chem. Soc.* **2003**, *125*, 1494. (b) Wang, J. C.; Liu, Q.; Liu, Q. F. *J. Mater. Chem.* **2005**, *15*, 4141. (c) Fang, Y. P.; Xu, A. W.; You, L. P.; Song, R. Q.; Yu, J. C.; Zhang, H. X.; Li, Q.; Liu, Z. Q. *Adv. Funct. Mater.* **2003**, *13*, 955. (d) Bai, X.; Song, H. W.; Pan, G. H.; Liu, Z. X; Lu, S. Z.; Di, W. H.; Ren, X. G.; Lei, Y. Q.; Dai, Q. L.; Fan, L. B. *Appl. Phys. Lett.* **2006**, *88*, 143104. (e) Tang, Q.; Liu, Z. P.; Li, S.; Zhang, S. Y.; Liu, X. M.; Qian, Y. T. *J. Cryst. Growth* **2003**, *259*, 208. (f) Zhang, J.; Liu, Z. G.; Lin, J.; Fang, J. *Cryst. Growth Des.* **2005**, *5*, 1527.

(36) (a) Wang, G.; Wang, Z. D.; Zhang, Y. X.; Fei, G. T.; Zhang, L. D. *Nanotechnology* **2004**, *15*, 1307. (b) Yu, L. X.; Song, H. W.; Liu, Z. X.; Yang, L. M.; Lu, S. Z. *Phys. Chem. Chem. Phys.* **2006**, *8*, 303. (c) Wan, J. X.; Wang, Z. H.; Chen, X. Y.; Mu, L.; Qian, Y. T. *J. Cryst. Growth* **2005**, *284*, 538. (d) Wu, X. C.; Tao, Y. R.; Gao, F.; Dong, L.; Hu, Z. *J. Cryst. Growth* **2005**, *277*, 643. (e) Wang, X.; Li, Y. D. *Chem. Eur. J.* **2003**, *9*, 5627.

(37) (a) Yang, J.; Quan, Z. W.; Kong, D. Y.; Liu, X. M.; Lin, J. *Cryst. Growth Des.* **2007**, *7*, 730. (b) Yang, J.; Lin, C. K.; Wang, Z. L.; Lin, J. *Inorg. Chem.* **2006**, *45*, 8973.

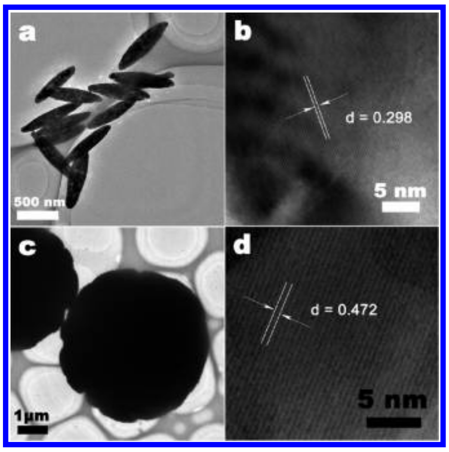

Figure 7. Typical TEM images of β-Ga_2O_3:3 mol % Dy^{3+} samples with (a) submicrospindle morphology (**P1′**) and (c) 3D hierarchical microsphere morphology (**P4′**), respectively. (b) and (d) are the corresponding HR-TEM images from a selected region.

of **P4′** is different from those of **P1′**− **P3′** samples. Figure 7d shows its *d* spacing as 0.472 nm, which corresponds to the distance between the (−201) planes.

In order to obtain the maximum luminescence intensity, we optimized the optimal doping concentration of Dy^{3+} ions in β-Ga_2O_3:$x$$Dy^{3+}$ samples. Figure S4 (Supporting Information) shows the PL intensity of Dy^{3+} as a function of the doping concentration (x) in β-Ga_2O_3:$x$$Dy^{3+}$ samples. The PL intensity of Dy^{3+} increases with an increase of its concentration (x) first, reaching a maximum value at 3 mol %, and then decreases with increasing concentration (x) due to the concentration quenching effect. Thus, the optimum concentration for Dy^{3+} is 3 mol % of Ga^{3+} in the Ga_2O_3 host and we choose β-Ga_2O_3:3 mol % Dy^{3+} as a "reference" compound for all characterizations. In general, the concentration quenching of luminescence is due to energy migration among the activator ions at high concentrations. In the energy migration process the excitation energy will be lost at a killer or quenching site, resulting in a decrease of PL intensity.

Under short-wavelength ultraviolet (UV) irradiation, the as-prepared GaOOH: 3 mol % Dy^{3+} samples do not show any luminescence due to the existence of large amount of OH groups, but β-Ga_2O_3 (denoted as **P3′-0**) and β-Ga_2O_3:3 mol % Dy^{3+} (**P3′**) samples with ellipsoid shape exhibit blue and near-white emission, respectively, and the corresponding photoluminescence photographs are shown in Figure S5 (Supporting Information). Figure 8a shows the PL excitation and emission spectra of **P3′-0** and **P3′**, respectively. The excitation spectrum for β-Ga_2O_3 (Figure 8a, left) contains a broad band from 220 to 280 nm with a maximum at 257 nm, which corresponds to the bandgap excitation.[38] Upon excitation at 257 nm, the emission spectrum of β-Ga_2O_3 contains a broad band from 370 to 580 nm with a maximum at 438 nm, as shown in Figure 8a (right), which is attributed to the recombination of an electron on a donor formed by oxygen vacancies with a hole on an acceptor formed by either gallium vacancies or gallium−oxygen vacancy pairs: namely, the transition of a self-activated optical center related to octahedrally coordinated GaO_6 groups.[38,39] In this case, the charge transfer occurs from the 2p orbital of O^{2-} to the empty 4s orbital of Ga^{3+}, since the 3d orbital is completely filled.[40] The excitation spectrum of **P3′** (Figure 8b, left black line) monitored with the 492 nm emission ($^4F_{9/2}$−$^6H_{15/2}$) of Dy^{3+} is basically identical with that of β-Ga_2O_3 (Figure 8a, left). It also consists of a broad band (220−280 nm) with a maximum at 257 nm. The presence of the excitation peak of the β-Ga_2O_3 host in the excitation spectrum of Dy^{3+} indicates that there is an energy transfer from the β-Ga_2O_3 host to Dy^{3+} ions in β-Ga_2O_3:3 mol % Dy^{3+}.[41] Excitation into the β-Ga_2O_3 host at 257 nm yields an emission spectrum corresponding to the f−f transitions of Dy^{3+}, which is dominated by two main groups of lines in the blue (460−520 nm) and yellow (560−610 nm) regions that correspond to the transitions from $^4F_{9/2}$ to $^6H_{15/2}$ and $^6H_{13/2}$ of Dy^{3+}, respectively.[38a,b,41] In comparison with the emission of Dy^{3+}, the intrinsic blue emission from the β-Ga_2O_3 host is very weak, indicating that an efficient energy transfer from the β-Ga_2O_3 host to Dy^{3+} has occurred. The energy transfer efficiency can be calculated according to the formula $\eta_{ET}=1-I_d/I_{d0}$, where I_d and I_{d0} are the corresponding

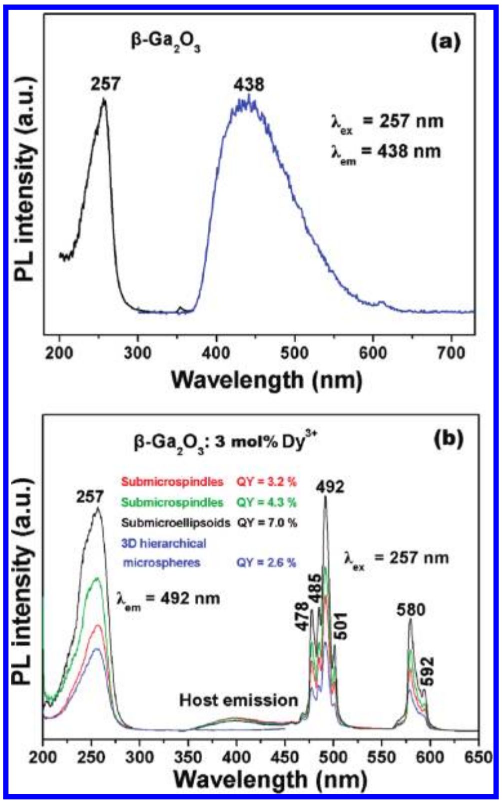

Figure 8. Photoluminescence excitation and emission spectra of (a) β-Ga_2O_3 (**P3′-0**) and (b) β-Ga_2O_3:3 mol % Dy^{3+} (**P3′**). The quantum yields of β-Ga_2O_3:3 mol % Dy^{3+} phosphors with different shapes are denoted by different colors in Figure 8b.

---

[38] (a) Pang, M. L.; Shen, W. Y.; Lin, J. *J. Appl. Phys.* **2005**, *97*, 033511. (b) Shen, W. Y.; Pang, M. L.; Lin, J.; Fang, J. *J. Electrochem. Soc.* **2005**, *152*, H25. (c) Sommerdijk, J. L.; Bril, A. *J. Electrochem. Soc.* **1975**, *122*, 952. (d) Herbert, W. C.; Minnier, H. B.; Brown, J. J. *J. Electrochem. Soc.* **1968**, *115*, 104. (e) Herbert, W. C.; Minnier, H. B.; Brown, J. J. *J. Electrochem. Soc.* **1969**, *116*, 1019. (f) Binet, L.; Gourier, D. *J. Phys. Chem. Solids* **1998**, *59*, 1241.

[39] Blasse, G.; Bril, A. *J. Inorg. Nucl. Chem.* **1967**, *29*, 266.

[40] Lakshminarasimhan, N. U.; Varadaraju, V. *Mater. Res. Bull.* **2006**, *41*, 724.

[41] Su, Q.; Pei, Z.; Lin, J.; Xue, F. *J. Alloys Compd.* **1995**, *225*, 103.

luminescence intensities of the donor (host lattice β-Ga_2O_3) in the presence and absence of the acceptor (doping rare earth ions, Dy^{3+}), respectively.[42] The energy transfer efficiencies from β-Ga_2O_3 to Dy^{3+} in β-Ga_2O_3:3 mol % Dy^{3+} are determined to be more than 90%.

In addition, Figure 8b also shows the excitation and emission spectra as well as quantum yield (QY) of β-Ga_2O_3:3 mol % Dy^{3+} phosphors with other shapes. It is found that the spectral profiles of **P3′** are basically similar to those of β-Ga_2O_3:3 mol % Dy^{3+} with other morphologies. This is because the excitation and emission of Dy^{3+} arise from f−f transitions which are strongly shielded by the outside 5s and 5p electrons. As a result, the excitation and emission spectra (peak positions) are not strongly dependent on the morphology of the Ga_2O_3 host lattices. However, the PL emission intensities of β-Ga_2O_3:3 mol % Dy^{3+} with the four different morphologies/sizes are different. Under identical measurement conditions, the relative intensities of the four samples are different: namely, the submicroellipsoid particles (black line) have the highest relative emission intensity, while the 3D hierarchical microsphere particles (blue line) show the lowest intensity, and the relative intensity of the former is more than 2 times as high as that of the latter. It is well-known that the surface area of materials increases along with a decrease in size. The large surface area introduces a large number of defects into the phosphor crystal. Defects have serious drawbacks in PL intensity for phosphors as they provide nonradiative recombination routes for electrons and holes. In order to be as efficient as possible for the phosphors, the number of electron/hole recombinations via optically active centers must be maximized. If the surface area is greatly reduced, a phosphor with fewer defects would show great improvement in the PL intensity.[43] Herein, the surface area of the as-synthesized **P3′** is smaller than those of **P1′** and **P2′** because **P3′** is greater in size than **P1′** and **P2′**. In addition, although the **P4′** sample had the largest size among the four samples, as shown in Table 1, the hierarchical structures of the **P4′** sample greatly increased its surface area, which made it have the lowest relative emission intensity. Therefore, a large number of electrons and holes in the excited state will return to the ground state via optically radiative recombination routes for submicroellipsoid phosphors. This is the reason that the PL intensity of β-Ga_2O_3:3 mol % Dy^{3+} submicroellipsoids is higher than that of β-Ga_2O_3:3 mol % Dy^{3+} submicrospindles and 3D hierarchical microspheres. Moreover, the measured absolute QY values of the **P1′**−**P4′** products are 3.2%, 4.3%, 7.0%, and 2.6%, respectively, in good agreement with the above emission intensity results.

A simple model illustrating the blue emission process in β-Ga_2O_3 and the energy transfer to Dy^{3+} is shown in Figure S6 (Supporting Information). Under UV excitation (257 nm, bandgap excitation), charge transfer from the O^{2-} ligand to the Ga^{3+} metal ion occurs, and then electrons (•) are excited from the valence band (VB) to the conduction band (CB) in β-Ga_2O_3. The excited levels of Ga^{3+} are $^4T_2$ (including $^4T_{2A}$, $^4T_{2B}$), $^4T_1$, and ^2E, and the ground state is $^4A_2$. After excitation, the electrons (•) move freely around the CB and finally relax to the donor band (oxygen vacancies): namely, the transitions from the $^4T_1$ excited level to the ground state $^4A_2$ occur, resulting in the blue emission at 438 nm.[39] When Dy^{3+} is present in β-Ga_2O_3 host lattices, the excitation energy can be nonradiatively transferred to Dy^{3+}, resulting in its characteristic emission.[38a,40]

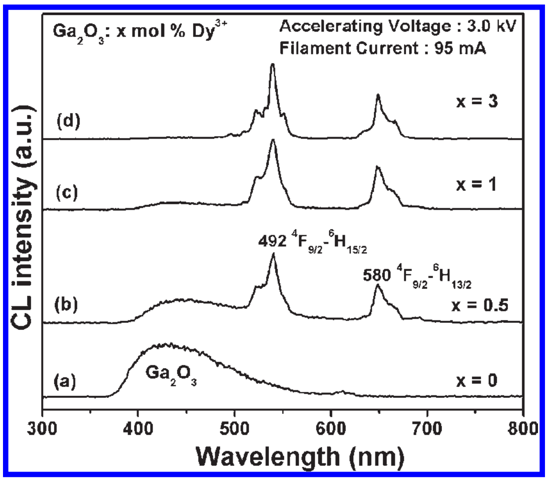

Figure 9. Emission spectra of the β-Ga_2O_3:x mol % Dy^{3+} submicroellipsoids with different concentrations (x = 0−3) under low-voltage electron beam excitation.

Under low-voltage electron beam excitation, the as-prepared **P3′-0** and **P1′-P4′** samples exhibit the same spectra profiles as their PL spectra, and their CL spectra are shown in Figure S7 (Supporting Information). Figure S7b shows the corresponding CIE chromaticity coordinates of **P3′-0** and **P1′-P4′** samples under electron beam excitation. They are located in the blue region for **P3′-0** (x = 0.1837, y = 0.1602), the near-white region for **P2′** (x = 0.2695, y = 0.3036) and **P4′** (x = 0.2558, 0.2903), and the white light region for **P1′** (x = 0.2841, 0.3104) and **P3′** (x = 0.2994, 0.3331), respectively. The representative CL photographs of **P3′-0** (blue light) and **P3′** (white light) are shown in the inset of Figure S7b. Furthermore, it can be seen from Figure S7a that the CL intensities of β-Ga_2O_3:0.03Dy^{3+} phosphors are related to their morphologies and sizes. Under low-voltage electron beam excitation, the **P3′** sample has the highest relative emission intensity, while the **P4′** sample shows the lowest intensity. This result is consistent with their PL spectra, and the reason is the same as in the description of PL. To further verify the existence of an energy transfer process from Ga_2O_3 to Dy^{3+} in β-Ga_2O_3:Dy^{3+}, Figure 9 shows the emission spectra of β-Ga_2O_3:x mol % Dy^{3+} (x = 0−3) with submicroellipsoid shape samples under 3.0 kV electron beam excitation. In the undoped β-Ga_2O_3, only the broad emission of Ga_2O_3 is observed. With the doping of Dy^{3+} (x = 0.5), in addition to Ga_2O_3 host emissions, we can also observe the characteristic emissions of Dy^{3+}. With an increase in Dy^{3+} concentration (x = 1, 3), the luminescence intensity of Ga_2O_3 decreases and that of Dy^{3+} increases due to the enhancement of the energy transfer probability from Ga_2O_3 to Dy^{3+} and is finally almost completely converted to the characteristic emission of Dy^{3+}. This result indicates

---

(42) Bourcet, J. C.; Fong, F. K. *J. Chem. Phys.* **1974**, *60*, 34.
(43) (a) Yang, J.; Liu, X. M.; Li, C. X.; Quan, Z. W.; Kong, D. Y.; Lin, J. *J. Cryst. Growth* **2007**, *303*, 480. (b) Yang, J.; Li, C. X.; Cheng, Z. Y.; Zhang, X. M.; Quan, Z. W.; Zhang, C. M.; Lin, J. *J. Phys. Chem. C* **2007**, *111*, 18148.

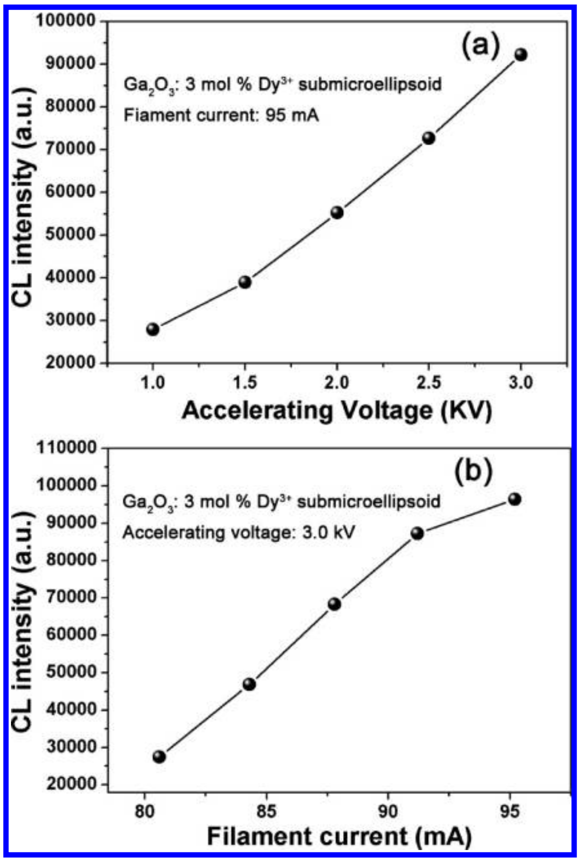

Figure 10. Cathodoluminescence intensities of a representative β-Ga$_2$O$_3$:3 mol % Dy^{3+} sample (**P3′**) as a function of (a) accelerating voltage and (b) filament current.

that there indeed is an efficient energy transfer from Ga$_2$O$_3$ to Dy^{3+} in β-Ga$_2$O$_3$:xDy^{3+} under low-voltage electron beam excitation.

The CL emission intensities of β-Ga$_2$O$_3$:3 mol % Dy^{3+} with ellipsoid-shaped (**P3′**) phosphors has been representatively investigated as a function of the accelerating voltage and the filament current, as shown in Figure 10. The results for **P1′, P2′**, and **P4′** samples are similar to that of **P3′** and will not be shown here. When the filament current is fixed at 90 mA, the CL intensity increases with an increase in the accelerating voltage from 1.0 to 3.0 kV (Figure 10a). Similarly, under a 3.0 kV electron-beam excitation, the CL intensity also increases with an increase in the filament current from 81 to 93 mA (Figure 10b). The increase in CL brightness with an increase in electron energy and filament current is attributed to the deeper penetration of the electrons into the phosphor body and the larger electron-beam current density. The electron penetration depth can be estimated using the empirical formula: $L\ (\text{Å}) = 250(A/\rho)(E/Z^{1/2})^n$, where $n = 1.2/(1 - 0.29 \log Z)$ and A is the atomic or molecular weight of the material, ρ is the bulk density, Z is the atomic number or the number of electrons per molecule in the case compounds, and E is the accelerating voltage (kV).[44] For **P3′**, $Z = 90$, $A = 193.0$, $\rho = 5.93$ g/cm^3, and the estimated electron penetration depth at 3.0 kV is about 3.4 nm. For CL, the Dy^{3+} ions are excited by the plasma produced by the incident electrons. The deeper the electron penetration depth, the more plasma will be produced, which results in more Dy^{3+} ions being excited and thus the CL intensity increases.

4. Conclusions

In summary, we have employed a facile homogeneous precipitation route to fabricate a series of GaOOH:Dy^{3+} samples with different morphologies, including submicrospindles, submicroellipsoids, and 3D hierarchical microspheres. Simplicity, low cost, ease of scale-up, diverse morphologies, and relative greenness (aqueous solution) constitute the key traits of this method. The experimental results demonstrate that the pH values in the initial reaction solution are responsible for the shape evolution of the GaOOH:Dy^{3+} products. These morphologies were formed from an initial phase of amorphous nanoparticles and subsequent anisotropic growth of the assembled crystallites at low pH, which was attributed to the selective absorption of OH$^-$ ions. After annealing at 1000 °C, GaOOH:Dy^{3+} can be easily converted to the resulting β-Ga$_2$O$_3$:Dy^{3+} phosphors. Under ultraviolet light and low-voltage electron beam excitation, the pure β-Ga$_2$O$_3$ host exhibits a blue emission with a maximum at 438 nm while the β-Ga$_2$O$_3$:Dy^{3+} samples show the characteristic emission of Dy^{3+} corresponding to $^4F_{9/2} \rightarrow {}^6H_{15/2,\ 13/2}$ transitions, indicating that there exists an efficient energy transfer from β-Ga$_2$O$_3$ to Dy^{3+}. Furthermore, the luminescence intensity of β-Ga$_2$O$_3$:Dy^{3+} is strongly related to their morphologies. Under UV and electron beam excitation, β-Ga$_2$O$_3$:Dy^{3+} phosphors with ellipsoid shapes show the highest emission intensity and QY among the four differently shaped samples due to the lowest surface defects, simultaneously giving a white emission. The CL intensity of the β-Ga$_2$O$_3$:Dy^{3+} phosphors increased with an increase in the accelerating voltage and filament current. On the basis of the above investigation, the as-prepared β-Ga$_2$O$_3$:Dy^{3+} phosphor has potential applications in FED and other photoelectric applications.

Acknowledgment. This project was financially supported by the National Basic Research Program of China (Grant Nos. 2007CB935502, 2010CB327704) and the National Natural Science Foundation of China (Grant Nos. NSFC 50702057, 50872131, 60977013, 20921002).

Supporting Information Available: Early growth stage of **P3** and **P4** samples (Figure S1), the PL intensity of Dy^{3+} ions as a function of its doping concentration (x) in β-Ga$_2$O$_3$:x mol % Dy^{3+} (Figure S4), FE-SEM images of **P1′**−**P4′** samples as well as the typical EDX spectrum of the **P3′** sample (Figure S2), TEM and HR-TEM images of **P2′** and **P3′** samples, respectively (Figure S3), photographs of **P3′-0**, **P1′**, and **P3′** samples under the irradiation of 254 nm UV light from a mercury lamp in a dark room (Figure S5), a simple model illustrating the blue emission process in β-Ga$_2$O$_3$ and the energy transfer process from β-Ga$_2$O$_3$ to Dy^{3+} (Figure S6), CL spectra and corresponding CIE chromaticity program of **P3′-0** and **P1′-P4′** samples and insets showing corresponding CL photographs of **P3′-0** and **P3′** samples (Figure S7). This material is available free of charge via the Internet at http://pubs.acs.org.

---

[44] Feldman, C. *Phys. Rev.* **1960**, *117*, 455.